Wideband single pixel feed system over 4.6-24 GHz for the Square Kilometre Array

Wideband single pixel feed system over 4.6–24 GHz for the Square Kilometre Array

Jonas Flygare
Onsala Space Observatory, SEE Dept.
Chalmers University of Technology
Gothenburg, Sweden
jonas.flygare@chalmers.se

Bin Dong
National Astronomical Observatories
Chinese Academy of Sciences
Chaoyang District, Beijing, China
dongbin@nao.cas.cn

Jian Yang
Dept. of Electrical Engineering
Chalmers University of Technology
Gothenburg, Sweden
jian.yang@chalmers.se

Leif Helldner
Onsala Space Observatory, SEE Dept.
Chalmers University of Technology
Gothenburg, Sweden
leif.helldner@chalmers.se

Magnus Dahlgren
Onsala Space Observatory, SEE Dept.
Chalmers University of Technology
Gothenburg, Sweden
magnus.dahlgren@chalmers.se

Jin Chengjin
National Astronomical Observatories
Chinese Academy of Sciences
Chaoyang District, Beijing, China
cjjin@nao.cas.cn

Miroslav Pantaleev
Onsala Space Observatory, SEE Dept.
Chalmers University of Technology
Gothenburg, Sweden
miroslav.pantaleev@gmail.com

Gary Hovey
Onsala Space Observatory, SEE Dept.
Chalmers University of Technology
Gothenburg, Sweden
gary.hovey@chalmers.se

John Conway
Onsala Space Observatory, SEE Dept.
Chalmers University of Technology
Gothenburg, Sweden
john.conway@chalmers.se

***Abstract*—We present the Band B feed system over 4.6–24 GHz designed for the Square Kilometre Array (SKA) reflector for radio astronomy applications. The feed is a Quad-ridge Flared Horn (QRFH) with a customized shape based on spline-defined profiles to achieve improved wideband performance. The feed system shows high aperture efficiency and sensitivity on the SKA reflector in predictions based on measured feed beam patterns. We present the feed design overview, cryogenic dewar concept and measurement of receiver noise (10–20 K) with wideband low-noise amplifiers, and full system simulation of the performance.**

***Index Terms*—quad-ridge flared horn, ultra-wideband feed, spine-defined profile, radio astronomy, sensitivity.**

I. Introduction

For high sensitivity observations with the next generation of radio telescopes, large collecting area and low system noise are needed. To achieve this, large single dish telescopes and large interferometric arrays are being constructed with highly optimized receivers. The receiver systems for large arrays of several hundreds of telescopes has a high total cost due to the large numbers needed, therefore it is advantageous to make them as capable as possible. Ultra-wideband (UWB) feed packages are of particular interest for their competitive noise temperature and large bandwidth [1], compact footprint for mid-sized reflectors, and reduced cost.

The Square Kilometre Array (SKA), will be the world's largest and most sensitivity radio telescope over its frequency range [2], with the first reflectors currently being constructed in South Africa. For the lowest frequencies of the SKA reflectors, 350–1050 MHz (Band 1), a 3:1 wideband feed system has been proposed and tested with successful result [3]. In order to cover the SKA Bands 3–5 (1.6–15.4 GHz) with a high-frequency extension of the baseline up to 24 GHz, a dual-feed dewar system is proposed. The system was developed under the Wide Band Single Pixel Feed (WBSPF) consortium in the SKA Advanced Instrumentation Programme (AIP). The two wideband feed packages within WBSPF, Band A (JLRAT/CETC54) and Band B (Onsala/Chalmers), are based on Quad-ridge Flared Horn (QRFH) technology covering 1.6–5.2 GHz and 4.6–24 GHz respectively. The Band B QRFH was developed using spline-defined profiles for UWB and high-frequency performance [4].

In this paper we present an overview of a proposed cryogenic feed system for the SKA Band B (4.6–24 GHz) with measured receiver noise and calculated observational sensitivity. The full reflector beam pattern and sensitivity is calculated by using measured feed beam patterns in a system simulator that implements physical optics (PO) and physical theory of diffraction (PTD). Average aperture efficiency for the feed is predicted to 70 % in the SKA reflector. The feed has low spill-over noise contribution in the SKA reflector which together with cryogenic low-noise amplifiers (LNA), delivered by Low Noise Factory (LNF), offers very low-noise performance over 5.2:1 bandwidth. Y-factor measurements indicate receiver noise temperature in the order of 15–20 K with the LNA accounting for 4–8 K noise.

Part of the project included in this publication has been funded by Swedish VR Research Infrastructures Planning Grant for Swedish contributions to the SKA radio-telescope in its pre-construction phase.

II. Feed Design

The Band B feed measures 202 mm in (aperture) diameter and 182 mm in length and is manufactured as four separate ridges and four separate horn quad-pieces, Fig. 1(c). The quad-pieces clamp the opposite ridges together for alignment, with a new edge-extrude feature to ensure good electrical contact [4]. The QRFH is intrinsically linearly dual-polarized and the Band B design is fed with two orthogonal single-ended 50 Ω coaxial ports inserted through one ridge and terminated in the opposite ridge for respective polarization. The measured reflection coefficient is lower than -10 dB over most of the band for both polarizations with an isolation of -25 dB (Fig. 7 in [4]).

A. Spline-defined Profile

The profiles of the horn and ridges of the Band B QRFH are constructed from numerical points splined together with one 'x' and 'z'-coordinate per point. The QRFH is separated in three different sections, one flared part mostly influencing the radiation performance, one impedance transition part from the 50 Ω feed point to the flared part, and a conically shaped backshort, see Fig. 1(a). The horn and ridge profile share the z-coordinate which reduces the total number of parameters in optimization. In Fig. 1(b), the total number of parameters for optimization in the feed is summarized to 60. Due to the separation of the feed in sections, individual parts could be optimized separately followed by a final optimization of all sections simultaneously. The advantage of a spline-defined profile is the customized shape that can improve the wideband performance compared to an analytic profile [4]. In Fig. 1(a), the initial shape of the Band B QRFH (left) is compared to the final optimized shape (right), where the special features of the profile (dashed highlights) is only achievable through spline-defined profiles. The feed was optimized for maximum aperture efficiency, η_a, and minimum reflection coefficient, S_{11}, across the band. The optimization was done in CST MWS connected to a MATLAB-script for calculation of η_a in an unshaped axial-symmetric reflector based on [5] to reduce iteration time. Physical optics and physical theory of diffraction simulations consistently predicted that 10 % higher η_a could be expected for Band B in the shaped SKA dual-reflector for which it is intended. In this way, the optimization time was reduced drastically and the degrees of freedom for the feed shape (with large number of spline-points) could be kept high.

B. Aperture Mode Content

The spline-defined profile of Band B produces a near-constant beamwidth over the frequency band and improved feed beam pattern symmetry. In [4] the aperture sub-efficiencies from a prime-focus simulation of the Band B feed are analyzed and show improvements compared to analytic QRFH profiles. The improved beam performance could be explained by the aperture mode content inside the horn, and we analyzed this for both

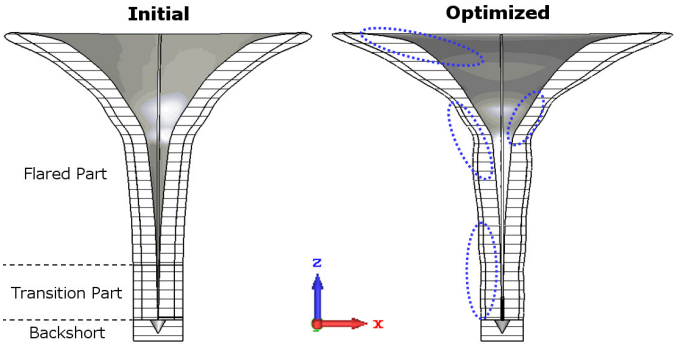

(a)

Flared Part:	Radiation	13 discrete points (38 parameters)
Transition Part:	Impedance Transform	6 discrete points (18 parameters)
Backshort, Ridge Thickness, Chamfer		4 parameters
Parameters in total: 60		

(b)

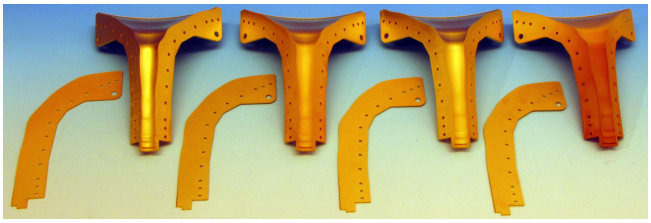

(c)

Fig. 1. (a) Band B QRFH cut showing initial (left) and optimized (right) shape of the spline-defined profiles; (b) Design parameter summary; (c) Manufactured ridges and quad-pieces before dewar integration.

TE modes and TM modes. The simulated E-field data at the feed aperture plane was extracted in CST MWS represented by (E_x, E_y, E_z), while the ideal fields TE_{mn} and TM_{mn}, represented by $(E_{x\mathrm{TEmn}}, E_{y\mathrm{TEmn}}, E_{z\mathrm{TEmn}})$ and $(E_{x\mathrm{TMmn}}, E_{y\mathrm{TMmn}}, E_{z\mathrm{TMmn}})$, were calculated with standard equations [6]. In total, 300 modes (m=1–10,n=1–15) have been calculated. A mathematical projection between the simulated QRFH E-field and each ideal mode was carried out to derive the corresponding coefficient according to

$$\mathrm{CO}_{\mathrm{TE}_{mn}} = \frac{E_x \cdot E_{x\mathrm{TEmn}} + E_y \cdot E_{y\mathrm{TEmn}} + E_z \cdot E_{z\mathrm{TEmn}}}{|E_x|^2 + |E_y|^2 + |E_z|^2} \tag{1}$$

$$\mathrm{CO}_{\mathrm{TM}_{mn}} = \frac{E_x \cdot E_{x\mathrm{TMmn}} + E_y \cdot E_{y\mathrm{TMmn}} + E_z \cdot E_{z\mathrm{TMmn}}}{|E_x|^2 + |E_y|^2 + |E_z|^2}. \tag{2}$$

Note that all the E-field values are normalized by its total power and the projections in (1) and (2) were done within a radius of 41.7 mm at the aperture plane, which is about the radius of an airy disk at 4.6 GHz. The magnitude (in percentage of total power) of the 13 most significant TE and TM modes are plotted in Fig. 2. Due to the magnetic-symmetrical

property of the quad-ridge structure, contents of all the even-order modes (i.e. $\mathrm{TE_{mn}}$ and $\mathrm{TM_{mn}}$ with m=0,2,4,...10) are almost zero and thus ignored for clarity. The results show that the $\mathrm{TE_{11}}$ mode is dominant at the lower band, but drops gradually towards higher frequency, where $\mathrm{TE_{12-13}}$ and $\mathrm{TM_{11-13}}$ are increasing. At high frequencies, the two major modes $\mathrm{TE_{11}}$ and $\mathrm{TM_{11}}$ show different proportions compared with the analysis in [7]. For the Band B, the $\mathrm{TE_{11}}$ content drops to less than 10 % while $\mathrm{TM_{11}}$ rises to 30 %. Besides that, contents of the other higher-order modes with $n > 3$ are suppressed to nearly zero, which demonstrates that only 3 TE modes ($\mathrm{TE_{11-13}}$) and 3 TM modes ($\mathrm{TM_{11-13}}$) are the main functional modes inside the horn. The spline-defined profiles provide a different management of the fundamental $\mathrm{TE_{11}}$ and $\mathrm{TM_{11}}$ modes, and are able to suppress the other higher-order modes to a larger extent, which results in an improved aperture efficiency.

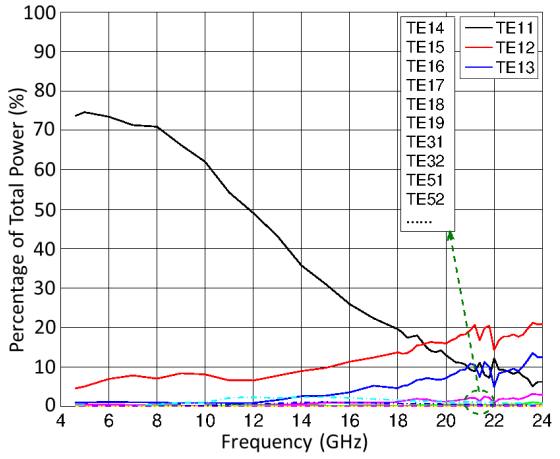

(a)

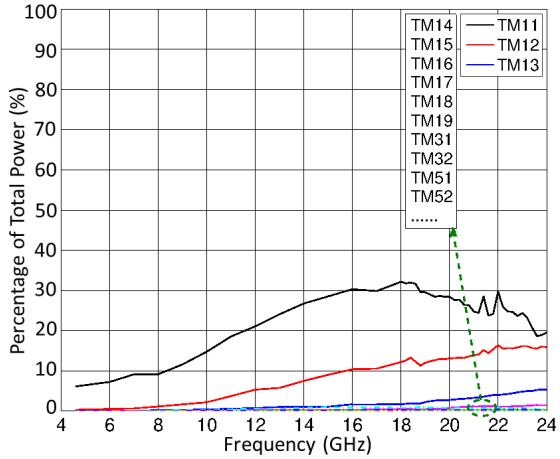

(b)

Fig. 2. The aperture mode content of the present Band B feed based on the simulated E-field data: (a) TE mode content; (b) TM mode content.

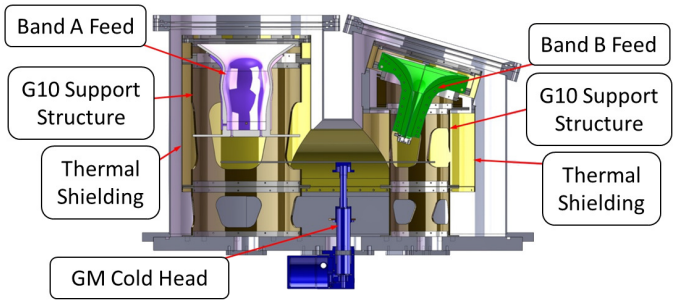

Fig. 3. Cross-section of the preliminary design for the SKA WBSPF cryostat.

III. Cryogenic Design and Measurement

A. Dual-feed Dewar

The dual-feed cryostat for SKA WBSPF aims to accommodate both Band A and Band B feeds and LNAs in a classical vacuum isolated dewar with a two-stage Gifford-McMahon closed cycle helium cryo-cooling system. In Fig. 3, a cross-section view is presented of the proposed dewar developed together with NAOC/JLRAT/TIPC, China. The main engineering requirements are:

- Place the feeds in dewar so that their respective phase center is located on the SKA dish feed-indexer's radius of rotation through the dish focal point.
- To match the SKA baseline helium supply system, a '2/9' cold head model from Oxford Cryosystems was chosen. The WBSPF feed package controller will use the same motor driver control-board as for SKA dish bands 2–5.
- Design for outdoor operation, keep mechanical interface towards the dish structure for maintenance.
- Compact design, consistent with agreed mechanical envelope limit set by the dish and adjacent feeds.
- Eliminate the risk of shadowing the optical path.

In addition to the engineering requirements listed above, the following performance requirements were taken in to account:

- Provide a temperature of 15 K at the LNAs and at most 80 K at the feed.
- Minimize ohmic loss along the signal path in the components preceding the LNA. Multi-layer Mylar is used to realize the vacuum window, to reduce the out-gassing and insertion loss compared to a Mylar/Foam combination.
- Minimize cryostat volume and internal surface areas for low out-gassing, long service life and low radiative thermal loading. Inner surface of the feeds are gold plated in order to further reduce thermal load and ohmic losses.
- Use vacuum compatible materials, minimize the length of the vacuum seals.

Considering compatibility to the current feed indexer, weight and manufacturability, the following structure was selected. The vacuum vessel consists of three modules: a central module that accommodates the cold head and the cold RF components and two cylinders allocated for the Band A and Band B feeds. The cryostat base plate at the bottom of the vacuum vessel

provides mechanical interface for the 2/9 cold head and the vacuum feed-throughs for the DC and RF cables as well for the pressure sensor and the vacuum valve. Each feed is surrounded by a 70 K radiation shield and has infrared filtering in front of the apertures. The overall dimensions of the cryostat (including sun shield and excluding the mounting mechanics) are: width of 1150 mm, depth of 600 mm and height of 750 mm. The weight of the cryostat is 164 kg. The phase centers of the two feeds are located on a 'circle' defined by the rotation radius of the feed indexer on the SKA dish for switching between the bands.

B. Receiver Noise Temperature Measurement

The estimated receiver noise temperature, T_{rec}, for Band B (4.6–24 GHz) is shown as a budget breakdown with each component's contribution in Table I. In addition, a 2 K 'general' contribution is made to the total noise budget accounting for dish, back-end and digitizer. The 1st stage UWB LNAs, provided by Low Noise Factory, are InP-based of single-ended topology with typical measured noise and gain of 6 K and 29 dB respectively. The dual-feed dewar described in Section III-A was not used for the T_{rec} tests described below, but rather a test dewar (housing one feed) with similar internal concept for cryogenic measurements. The layout of the dewar used for measurements is presented in Fig. 4(b). The standard approach with Y-factor measurement was used with a hot and cold load ([6], pp. 501). Ambient temperature absorbers were used as the hot load, T_{hot}, where the temperature was determined with a probe thermometer. The sky was used as the cold load, T_{cold}, and measurements of the output power for the receiver under respective load gives the Y-factor as $Y = P_{\text{hot}}/P_{\text{cold}} = (T_{\text{hot}} + T_{\text{rec}})/(T_{\text{cold}} + T_{\text{rec}}) > 1$. For T_{cold} the general SKA-model was used [8], with corrections added for the large variations in attenuation level at high frequencies around the water-vapor line at 22 GHz. The tests were performed at Onsala Space Observatory, so the correction data are calculated from water-vapor radiometry (WVR) data for the site (located next to the ocean) during the period of measurement. The uncertainty at mid and high frequencies in the result is estimated to be in the order of a few Kelvin. Known radio frequency interference (RFI) was removed from the final result. Resulting T_{rec} is presented in Fig. 4(a) together with a stand-alone measurement of T_{LNA} and the estimated value of T_{rec} corresponding to the noise-budget breakdown presented in Table I. The larger ripple in the low and high frequencies is most likely due to mismatch between the feed and LNA causing a standing-wave degradation of the performance. The test dewar was not optimized in terms of window size relative to the feed aperture location. This could contribute to the resonant behavior for this type of wide-beam feeds as well. In the dual-feed dewar this design criterion is specifically addressed to mitigate possible uncertainty.

TABLE I
ESTIMATED RECEIVER NOISE BUDGET FOR SKA BAND B

Noise Component	Loss (dB)	T_{phy} (K)	Noise (K)
Vacuum window	0.04	300	2.78
IR-filter 1st	0.015	200	0.70
IR-filter 2nd	0.015	150	0.52
Feed ohmic loss	0.08	50	0.94
Feeding line loss	0.1	20	0.48
Directional coupler	0.3	20	1.52
LNA		20	6.81
General noise			2.00
Total Noise (K)			$\mathbf{15.75(\pm 2)}$

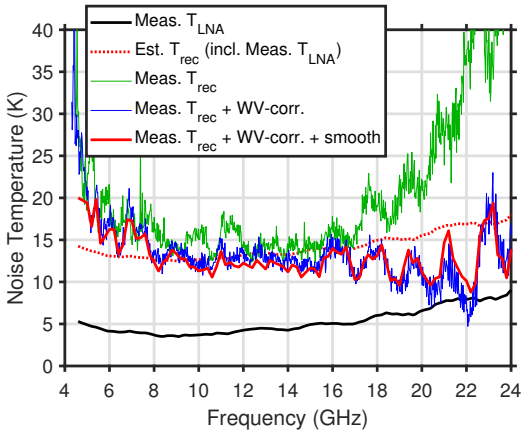

(a)

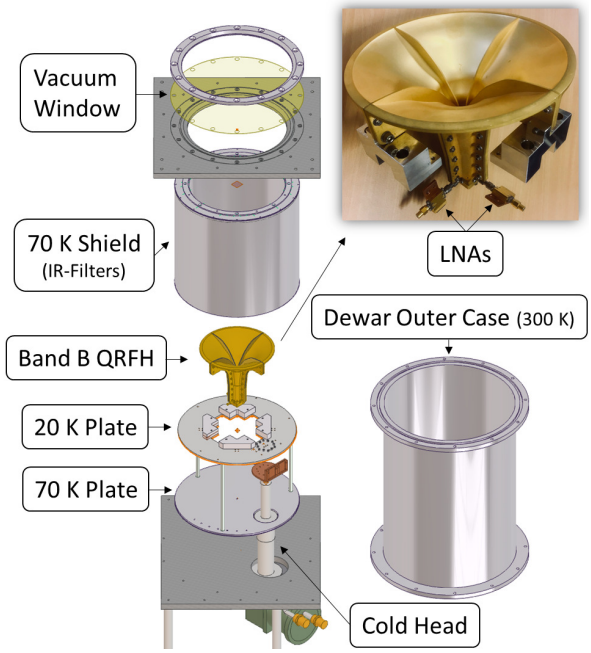

(b)

Fig. 4. (a) Measured receiver noise temperature of the Band B system; (b) Test dewar layout for cryogenic measurement, and a photo of the feed and LNAs before assembly.

IV. Simulated Performance in SKA Reflector

A. System Simulation

To properly evaluate the system performance in the design reflector (SKA, shaped offset-Gregorian [9]), a system simulator was used to calculate the full reflector beam pattern,

antenna noise temperature T_a, and cross-polarization performance [10]. In the system simulator, the reflector geometry is illuminated with the feed beam pattern (simulated or measured) and through the PO and PTD tools of TICRA GRASP, the full reflector beam pattern is calculated. This pattern is then integrated, weighted by the SKA general brightness temperature model [8], for an accurate calculation of T_a which includes the spill-over noise. It was shown for the SKA Band 1 that excellent agreement between simulation and measurement was achieved using this approach [3]. In the results shown below, the measured Band B feed beam pattern was used in the system simulator to illuminate the reflector geometry.

B. Aperture Efficiency

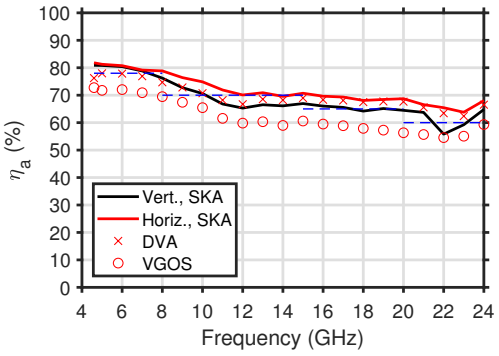

Fig. 5. Predicted aperture efficiency, η_a, for the Band B feed calculated in SKA, DVA, and VGOS reflector. Two polarizations are shown for the SKA reflector, dashed blue lines indicate target efficiency for resp. frequency interval in the band. Measured feed beam patterns were used to calculate reflector beam patterns.

The Band B feed design has predicted aperture efficiency, η_a, in the SKA reflector better than 78 %, 70 %, 65 %, and 60 % over frequency intervals 4.6–8 GHz, 8–15 GHz, 15–20 GHz, and 20–24 GHz respectively. The vertical polarization on the reflector show slightly lower efficiency. This difference is not caused by the feed beam patterns, which are identical for the two orthogonal polarizations, but rather the resulting sub-reflector field taper illuminating the main reflector. The sensitivity figure-of-merit is proportional to η_a and is therefore also affected as seen in Fig. 6. This is a property not seen at low frequencies and can be compensated for in high-frequency QRFH by an asymmetric design [11]. In Fig. 5, the predicted aperture efficiency using measured feed beam patterns from Band B is presented for the shaped SKA reflector as well as for the SKA precursor reflector DVA [12], and the VGOS reflector (unshaped) for next generation of geodetic VLBI stations [13]. All three reflectors have similar half-subtended angle (SKA: θ_e=58°) and the ∼10 % reduction of η_a in the VGOS reflector is because it is unshaped. The calculations assume perfect surface on the reflectors.

C. Sensitivity

The figure-of-merit for a radio telescope system is the sensitivity, here presented as

$$\frac{A_{\text{eff}}}{T_{\text{sys}}} \tag{3}$$

where A_{eff} is the effective area in square meters (proportional to η_a) and T_{sys} is the system noise temperature in Kelvin. The major contributions to T_{sys} is T_{rec} and T_a. A higher value in (3) implies a more sensitive telescope for observation. The predicted sensitivity presented here is calculated with the system simulator described in Section IV-A. For the frequency range 4.6–16 GHz the contribution from T_a to T_{sys} is 6–12 K, and above 16 GHz the water-line (22 GHz) highly attenuates the signal. This results in a decreasing sensitivity as the frequency increases in Fig. 6(a), where also the brightness temperature of the sky is presented (T_b). In T_{sys} the measured T_{rec}, presented in Fig. 4(a), is included and therefore there is a ripple in the sensitivity curves. The result in Fig. 6(b) shows the sensitivity over zenith angle, θ_p, presented for two frequencies when the telescope is tipping away from zenith (θ_p=0°). The performance is rather stable over the SKA-

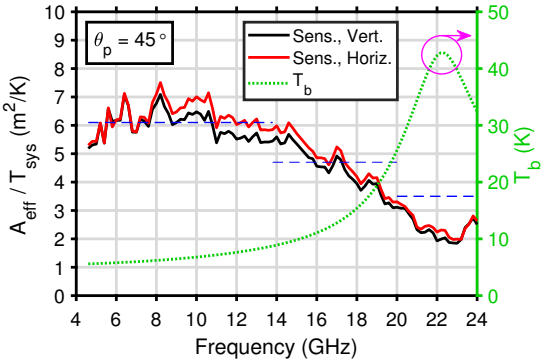

(a)

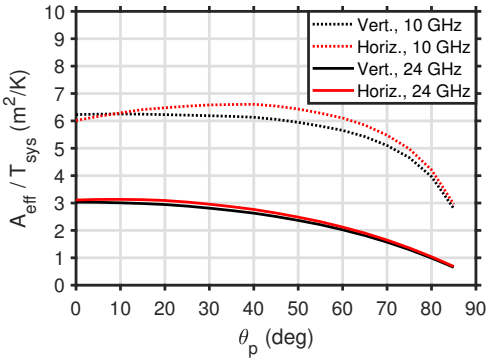

(b)

Fig. 6. Predicted sensitivity, $A_{\text{eff}}/T_{\text{sys}}$, for the Band B feed calculated in SKA reflector using measured T_{rec} data (Fig. 4(a)). (a) Sensitivity over frequency for θ_p=45°, green dotted curve show sky brightness temperature T_b. Dashed blue lines indicate target sensitivity for resp. frequency interval in the band; (b) Sensitivity over zenith angle (θ_p) for 10 GHz and 24 GHz. Measured feed beam patterns were used to calculate reflector beam patterns.

specified interval $\theta_{\mathrm{p}} \in [0^\circ, 60^\circ]$. This is due to high spill-over efficiency with the optimized feed, and the additional 40° spill-over shield on the bottom-part of the SKA sub-reflector. The SKA reflector is in feed-down configuration meaning that the sub-reflector moves closer to the ground as the telescope is pointing it's main beam closer to the horizon. The spill-over shield significantly reduces the noise picked up from ground, even as θ_{p} increases. This effect combined with the difference in η_{a} causes 'separation' between the polarization's sensitivity curves over θ_{p} in Fig. 6(b).

V. Conclusions

The wideband feed package presented in this paper over 4.6–24 GHz has high sensitivity over low and mid band with high aperture efficiency across all frequencies. The Band B high-frequency system covers the SKA baseline Band 5, and extends it up to K-band with applications in both radio astronomy and geodetic VLBI observations due to mutual frequency bands of interest. From Y-factor tests, the receiver noise is measured to 10–20 K across the band. The spline-defined profiles of the Band B QRFH improves the feed beam symmetry over a large bandwidth (5.2:1) as well as the spill-over efficiency.

Acknowledgment

The authors would like to thank Low Noise Factory, Sweden for their dedicated contributions to the SKA project. The system simulator was provided by Marianna Ivashina in the antenna group of the electrical engineering department at Chalmers University of Technology, Sweden.

References

[1] S. Weinreb, H. Mani, W. Zhong, J. Flygare, B. Billade, A. Akgiray, and L. Dong, "Cryogenic 1.2 to 116 GHz Receiver for Large Arrays," in *Proc. 12th Euro. Conf. Antennas Propag. (EuCAP 2018)*, London, UK, Apr. 2018.

[2] P. E. Dewdney, W. Turner, R. Braun, J. Santander-Vela, M. Waterson, and G. Tan, "SKA1 System Baseline V2 Description (SKA-TEL-SKO-0000308)," Nov. 2015. [Online]. Available: https://www.skatelescope.org/wp-content/uploads/2014/11/SKA-TEL-SKO-0000002-AG-BD-DD-Rev01-SKA1_System_Baseline_Design.pdf

[3] J. Flygare, A. Peens-Hough, L. Helldner, M. Dahlgren, G. Smit, P. Kotze, R. Wingdén, T. D. Carrozi, U. Kylenfall, L. Pettersson, and M. Pantaleev, "Sensitivity simulation and measurement of the SKA Band 1 wideband feed package on MeerKAT," in *Proc. 13th Euro. Conf. Antennas Propag. (EuCAP 2019)*, Krakow, Poland, Apr. 2019.

[4] B. Dong, J. Yang, J. Dahlström, J. Flygare, M. Pantaleev, and B. Billade, "Optimization and Realization of Quadruple-ridge Flared Horn with New Spline-defined Profiles as a High-efficiency Feed over 4.6-24 GHz," *IEEE Trans. Antennas Propag.*, vol. 67, no. 1, pp. 585–590, 2019.

[5] P.-S. Kildal, "Factorization of the feed Efficiency of Paraboloids and Cassegrain Antennas," *IEEE Trans. Antennas Propag.*, vol. 33, no. 8, pp. 903–908, 1985.

[6] D. M. Pozar, *Microwave Engineering*, 4th ed. Wiley, 2012.

[7] A. Akgiray, S. Weinreb, W. A. Imbriale, and C. Beaudoin, "Circular quadruple-ridged flared horn achieving near-constant beamwidth over multioctave bandwidth: Design and measurements," *IEEE Trans. Antennas Propag.*, vol. 61, no. 3, pp. 1099–1108, Mar. 2013.

[8] G. Cortes-Medellin, "MEMO 95 Antenna noise temperature calculation," pp. 1–13, Jul. 2007. [Online]. Available: https://www.skatelescope.org/uploaded/6967_Memo_95.pdf

[9] R. Lehmensiek, I. P. Theron, and D. I. De Villiers, "Deriving an Optimum Mapping Function for the SKA-Shaped Offset Gregorian Reflectors," *IEEE Trans. Antennas Propag.*, vol. 63, no. 11, pp. 4658–4666, 2015.

[10] M. V. Ivashina, O. Iupikov, R. Maaskant, W. A. Van Cappellen, and T. Oosterloo, "An optimal beamforming strategy for wide-field surveys with phased-array-fed reflector antennas," *IEEE Trans. Antennas Propag.*, vol. 59, no. 6, pp. 1864–1875, 2011.

[11] B. Dong, J. Yang, M. Pantaleev, J. Flygare, and B. Billade, "Design of an Asymmetrical Quadruple-ridge Flared Horn Feed : a Solution to Eliminate Polarization Discrepancy in the Offset Reflecting Systems," in *Proc. 12th Euro. Conf. Antennas Propag. (EuCAP 2018)*, London, UK, Apr. 2018.

[12] L. B. G. Knee, L. A. Baker, A. D. Gray, G. J. Hovey, M. J. Kesteven, G. Lacy, and T. Robishaw, "System performance testing of the DVA1 radio telescope," in *Proc. SPIE 9906, Ground-based and Airborne Telescopes VI*, H. J. Hall, R. Gilmozzi, and H. K. Marshall, Eds., no. July 2016, jul 2016, p. 99063T.

[13] A. Niell, J. Barrett, A. Burns, R. Cappallo, B. Corey, M. Derome, C. Eckert, P. Elosegui, R. McWhirter, M. Poirier, G. Rajagopalan, A. Rogers, C. Ruszczyk, J. SooHoo, M. Titus, A. Whitney, D. Behrend, S. Bolotin, J. Gipson, D. Gordon, E. Himwich, and B. Petrachenko, "Demonstration of a Broadband Very Long Baseline Interferometer System: A New Instrument for High-Precision Space Geodesy," *Radio Science*, no. May, pp. 1–23, 2018.